

Extended quantum critical phase in a magnetized spin- $\frac{1}{2}$ antiferromagnetic chain

M. B. Stone,^{1,*} D. H. Reich,¹ C. Broholm,^{1,2} K. Lefmann,³ C. Rischel,⁴ C. P. Landee,⁵ and M. M. Turnbull⁵

¹*Department of Physics and Astronomy, Johns Hopkins University, Baltimore, Maryland 21218*

²*National Institute of Standards and Technology, Gaithersburg, MD 20899*

³*Materials Research Department, Risø National Laboratory, DK-4000 Roskilde, Denmark*

⁴*Ørsted Laboratory, Niels Bohr Institute, University of Copenhagen, DK-2100, København Ø, Denmark*

⁵*Carlson School of Chemistry and Department of Physics, Clark University, Worcester, MA 01610*

(Dated: February 25, 2018)

Measurements are reported of the magnetic field dependence of excitations in the quantum critical state of the spin $S = 1/2$ linear chain Heisenberg antiferromagnet copper pyrazine dinitrate (CuPzN). The complete spectrum was measured at $k_B T/J \leq 0.025$ for $H = 0$ and $H = 8.7$ Tesla where the system is $\sim 30\%$ magnetized. At $H = 0$, the results are in quantitative agreement with exact calculations of the dynamic spin correlation function for a two-spinon continuum. At high magnetic field, there are multiple overlapping continua with incommensurate soft modes. The boundaries of these continua confirm long-standing predictions, and the intensities are consistent with exact diagonalization and Bethe Ansatz calculations.

PACS numbers: 75.10.Jm, 75.40.Gb, 75.50.Ee

One of the most important ideas to emerge from studies of condensed matter systems in recent years is the concept of quantum criticality [1]. A quantum critical point marks a zero temperature phase transition between different ground states of a many-body system as a result of changes in parameters of the underlying Hamiltonian. Precisely at the quantum critical point the system is without characteristic length scales or energy scales, with power-law spatial correlations and gapless excitations. Finite temperature properties close to quantum criticality are anomalous and reflect universal properties of the underlying quantum field theory.

While fine tuning of a parameter in a system's Hamiltonian is generally required to achieve quantum criticality, it is inherent to the spin $S=1/2$ linear chain Heisenberg antiferromagnet (LCHAFM). The spin dynamics of the LCHAFM have been studied in a number of materials [2, 3, 4, 5, 6], and the elementary excitations are $S=1/2$ spinons that form a gapless, two-particle continuum [7, 8]. In a magnetic field, H the Hamiltonian of the LCHAFM is $\mathcal{H} = \sum_i [J\mathbf{S}_i\mathbf{S}_{i+1} - g\mu_B H S_i^z]$. While changes in \mathcal{H} such as the introduction of dimerization or interchain coupling drive the LCHAFM away from criticality [9], the system should remain quantum critical at $T = 0$ in fields below the fully spin polarized state, which occurs at $H_C = 2J/g\mu_B$ [10, 11]. Prominent among the features predicted to exist along this quantum critical line are a set of field-dependent two-particle continua [7, 12, 13, 14] with incommensurate soft modes that move across the 1D Brillouin zone with increasing field as $\tilde{q}_{i,1} = 2\pi m$ and $\tilde{q}_{i,2} = \pi - 2\pi m$, where $0 \leq m \leq 1/2$ is the reduced magnetization per spin.

Experiments on copper benzoate [15] have verified the predicted field-dependence of the incommensurate wavevector $\tilde{q}_{i,2}$. However, due to a combination of a staggered g -tensor and Dzyaloshinskii-Moria interactions,

the field drives that system away from the critical line to a state with confined spinons and a gap in the excitation spectrum [16]. In contrast, the finite-field critical state of the $S=1/2$ LCHAFM is accessible in copper pyrazine dinitrate, $\text{Cu}(\text{C}_4\text{H}_4\text{N}_2)(\text{NO}_3)_2$ (CuPzN). This well characterized organo-metallic magnet has $J = 0.9$ meV, and negligible interchain coupling ($J'/J < 10^{-4}$) [6, 17]. The spin chains in CuPzN are uniform, with one Cu^{2+} ion per unit cell along the chain, and specific heat measurements have shown that CuPzN remains gapless for $H \leq 0.6H_C = 9$ T [6]. In this paper we report inelastic neutron scattering measurements of the full spectrum of CuPzN, both at $H = 0$ and at $H = 8.7$ T, where $m = 0.15$. In zero field, the spectrum is consistent with the exact two-spinon contribution to the spin fluctuation spectrum [8]. The finite field data show the long-sought field-dependent continua [7], and are in detailed agreement with theoretical and numerical work [12, 13, 14].

The measurements were performed using the SPINS cold neutron triple axis spectrometer at the NIST Center for Neutron Research. The sample studied contained 22 single crystals of deuterated CuPzN [18] with a total mass of 3.06 grams, and a measured mosaic of two degrees. We used a dispersive analyzer configuration that detects scattered neutrons with an angular range of 10° and an energy range $2.7 \text{ meV} \leq E_f \leq 3.55 \text{ meV}$ [19]. We used a Be filter before the sample for $E_i < 5.15$ meV, and a BeO filter after the sample. The measured full width at half maximum (FWHM) elastic energy resolution was $\delta\hbar\omega = 0.14$ meV, and the FWHM wave-vector resolution along the [100] chain axis was $\delta\mathbf{Q}_\parallel = 0.03 \text{ \AA}^{-1}$ at $\mathbf{Q} = (hkl) = (\frac{3}{2}\frac{1}{4}0)$ at $\hbar\omega = 0$ [20]. Data were obtained along the line between $\mathbf{Q} = (1\frac{1}{4}0)$ and $\mathbf{Q} = (2\frac{1}{4}0)$, with $H \parallel \hat{c}$.

Figure 1(a) shows the normalized magnetic scattering intensity $\tilde{I}_m(\tilde{q}, \omega)$ for CuPzN, measured in zero field at

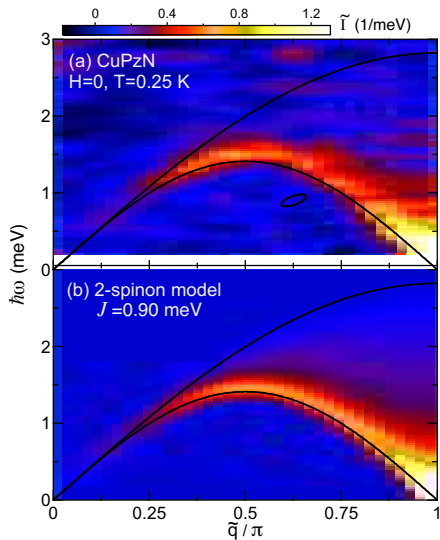


FIG. 1: (a) Magnetic inelastic neutron scattering intensity \tilde{I}_m for CuPzN at $T = 0.25$ K and $H = 0$ versus wave-vector and energy transfer. (b) Calculated two-spinon contribution to \tilde{I}_m . Solid lines are the predicted lower and upper bounds of the spinon continuum. A representative FWHM resolution ellipsoid is shown in (a).

$T = 0.25$ K. Wave-vector transfer along the chain is represented as $\tilde{q} = 2\pi(h - 1)$. This data set was obtained by combining data taken at $E_i = 3.35$ meV, 3.55 meV, and for 3.75 meV $\leq E_i \leq 5.75$ meV with 40 μ V steps. After subtracting the background scattering measured with the analyzer in a non-reflecting geometry, the incoherent elastic scattering profile of the sample was determined from data that were at least 0.2 meV outside of the known bounds [6] of the $H = 0$ spinon continuum. This profile was scaled to the measured elastic incoherent scattering intensity at each \tilde{q} , and subtracted from the raw data. The data were converted to the normalized scattering intensity by comparison with the measured incoherent scattering intensity of a vanadium standard. The data at $2\pi - \tilde{q}$ were then averaged with that at \tilde{q} , binned in bins of size $\delta\hbar\omega = 25$ μ eV by $\delta\tilde{q} = 0.026\pi$, and averaged over a rectangle of the same size as the FWHM energy and wave-vector resolutions to produce the color contour plot shown in Fig. 1(a).

These data provide a complete picture of the zero-field spinon continuum (SC) in CuPzN. The solid lines are the SC's lower and upper bounds, calculated for $J = 0.9$ meV [7]. Figures 3(a)-(c) and 2(a)-(c) show cuts through the data, and highlight several important features. These include the monotonically decreasing intensity at $\tilde{q} = \pi$ [Fig. 2(a)], the peaks near $\tilde{q} = \pi$ associated with the divergence in $\mathcal{S}(\tilde{q}, \omega)$ at the SC lower bound [8] [Fig. 3(a)-(c)], and the smaller feature at low \tilde{q} where the SC narrows as $\tilde{q} \rightarrow 0$. Figures 2(b)-(c) show the asymmetric

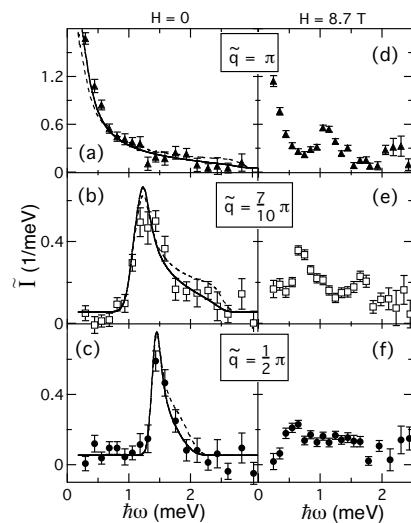


FIG. 2: Magnetic scattering intensity vs $\hbar\omega$ at constant \tilde{q} for CuPzN at $T = 0.25$ K and $H = 0$ (a)-(c), and at $H = 8.7$ T (d)-(f). Each point includes scattering within a width of $\Delta\tilde{q} = 0.05\pi$. The solid (dashed) lines in (a)-(c) are the exact (approximate) model for $\mathcal{S}(\tilde{q}, \omega)$ described in the text.

lineshapes produced by the SC for $\tilde{q} \neq \pi$. Figure 3(c) also shows data taken at $T = 35$ K. The decrease in intensity at $\tilde{q} = \pi$ confirms that the low- T scattering is magnetic.

Figure 1(b) shows $\tilde{I}_m(\tilde{q}, \omega)$ calculated [6] from the recently derived exact two-spinon contribution to $\mathcal{S}(\tilde{q}, \omega)$ [8, 21, 22] with $J = 0.9$ meV, with the addition of a constant intensity fixed at the average residual background measured 0.5 meV away from the continuum. $\tilde{I}_m(\tilde{q}, \omega)$ is also shown as solid lines on the cuts in Figs. 3(a)-(c) and 2(a)-(c). There are no adjustable parameters in the model, and the agreement with the data is excellent, although we note that there is an overall 10% uncertainty in the vanadium normalization.

Figures 3 and 2 also show a comparison (dashed lines) to the lineshapes produced by a global fit to the approximate form [7] for $\mathcal{S}(\tilde{q}, \omega)$ that has been previously used to model measurements of the $H = 0$ SC in CuPzN [6] and other materials [2, 3]. This approximation is now known to overestimate $\mathcal{S}(\tilde{q}, \omega)$ near the upper SC boundary [8, 12]. Indeed, some indications of this effect are seen in Figs. 2(b) and 2(b), and although our data are not optimal for observing these differences, the exact model does give an overall better description of the data.

The spectrum of CuPzN in a magnetic field is considerably more complex than at zero field, as seen in Fig. 4(a), which shows \tilde{I}_m measured at $H = 8.7$ T. This data set combines data taken in the range 3.35 meV $\leq E_i \leq 4.75$ meV with 20 μ V increments, and at $E_i = 5.15$ meV. An identical background subtraction, averaging, and binning procedure as used at $H = 0$ was applied to these data,

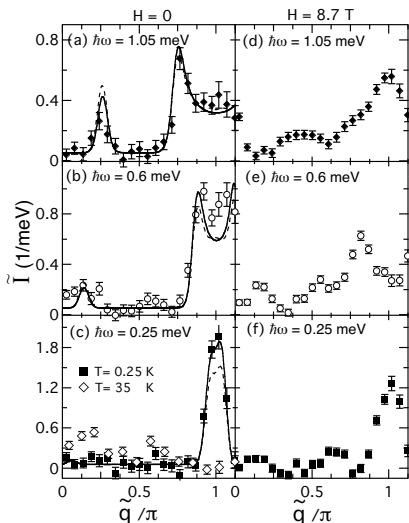


FIG. 3: Magnetic scattering intensity vs \tilde{q} at constant $\hbar\omega$ for CuPzN at $T = 0.25$ K at $H = 0$ (a)-(c), and at $H = 8.7$ T (d)-(f). The data for $\tilde{q} < \pi$ have been averaged with the data at $2\pi - \tilde{q}$. The data displayed for $\tilde{q} > \pi$ have not been averaged in this manner. Each point includes scattering within a width of $\Delta\hbar\omega = 0.1$ meV. The solid (dashed) lines in (a)-(c) are the exact (approximate) model for $\mathcal{S}(\tilde{q}, \omega)$ described in the text. The scattering measured at $T = 35$ K is shown as open symbols in panel (c).

using the $H = 0$ incoherent elastic profile.

Several continua and prominent features have emerged that were not present at $H = 0$. These are highlighted in cuts shown in Figs. 3(d)-(f) and 2(d)-(f). First, a continuum of scattering is still observed at $\tilde{q} = \pi$ down to the lowest energy probed, which demonstrates that the system indeed remains gapless and critical at $H = 8.7$ T. The spectrum has generally shifted to lower energy, and the strong ridge of scattering with linear dispersion near $\tilde{q} = \pi$ has a smaller slope than at $H = 0$, showing explicitly that the velocity of the elementary excitations has decreased [6].

There is a strong peak in $\tilde{\mathcal{I}}_m(\tilde{q}, \omega)$ centered at $\tilde{q} = \pi$ at the field energy $\hbar\omega = g\mu_B H \approx 1.1$ meV ($g_c = 2.07$ [23]). A weaker peak at this same energy can also be seen at $\tilde{q} = 0$, which corresponds to uniform spin precession. Moving away from $\tilde{q} = \pi$, there is another ridge of scattering intensity, which decreases in energy towards the expected field induced incommensurate wavevector $\tilde{q}_{i,2} = 0.7\pi$. As shown in Fig. 2(e), the incommensurate mode is seen in increased scattering at the lowest energies probed at $\tilde{q}_{i,2}$ compared to zero field [Fig. 2(b)]. Finally, there is a mode that begins at the field energy at $\tilde{q} = 0$, and decreases in energy with increasing \tilde{q} , but which loses intensity close to $\tilde{q}_{i,1} = 0.3\pi$, consistent with numerical work [12].

Using the Bethe Ansatz, Müller *et al.* identified six classes of excitations out of the partially magnetized

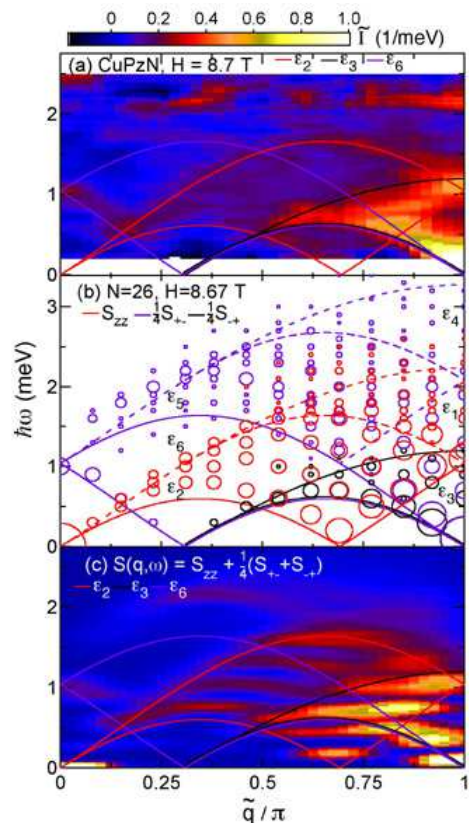


FIG. 4: (a) Inelastic neutron scattering intensity $\tilde{\mathcal{I}}_m(\tilde{q}, \omega)$ for CuPzN at $T = 0.25$ K and $H = 8.7$ T. (b) Calculations of the different components of $\mathcal{S}(\tilde{q}, \omega)$ for $N = 26$ spins and $m = 2/13$ ($H = 8.67$ T for CuPzN). The area of each circle is proportional to $\mathcal{S}(\tilde{q}, \omega)$. (c) $\tilde{\mathcal{I}}_m(\tilde{q}, \omega)$ calculated for ensemble of chains with $N = 24, 26$, and 28 . Lines show bounds of excitation continua for the finite-length $S = 1/2$ LCHAFM. Solid lines: continua predicted to predominate as $N \rightarrow \infty$.

ground state of an N -spin chain that can contribute to $\mathcal{S}(\tilde{q}, \omega)$ [7]. Each class produces a continuum, and Müller *et al.* determined their approximate boundaries. However, three of these are predicted to dominate $\mathcal{S}(\tilde{q}, \omega)$ as $N \rightarrow \infty$, with (adopting the notation of Ref. [7],) class (ii) contributing to $\mathcal{S}_{zz}(\tilde{q}, \omega)$, class (iii) to $\mathcal{S}_{-+}(\tilde{q}, \omega)$, and class (vi) to $\mathcal{S}_{+-}(\tilde{q}, \omega)$. The boundaries of these three continua, \mathcal{E}_2 , \mathcal{E}_3 , and \mathcal{E}_6 , are shown as solid lines in Fig. 4. They closely track the principal features of the data.

We have calculated $\mathcal{S}(\tilde{q}, \omega)$ for chains of length $N = 24, 26$, and 28 , using the Lanczos technique [12]. Figure 4(b) depicts the results for $N = 26$ and $m = 2/13$, corresponding to $H = 8.67$ T for CuPzN [7]. Each eigenstate of the chain is marked by a circle with an area proportional to the corresponding contribution to $\mathcal{S}(\tilde{q}, \omega)$ [12]. The circles are color-coded to indicate which component of $\mathcal{S}(\tilde{q}, \omega)$ the state contributes to. Note that in our experimental geometry we measure $\tilde{\mathcal{I}}_m(\tilde{q}, \omega) \propto \mathcal{S}_{zz} + \frac{1}{4}(\mathcal{S}_{+-} + \mathcal{S}_{-+})$. The corresponding continuum boundaries are also shown color-coded. Some spectral

weight for this finite chain is seen outside of continua (ii), (iii) and (vi), and so for reference the boundaries of the other three finite- N continua, \mathcal{E}_1 , \mathcal{E}_4 , and \mathcal{E}_5 , are included as dashed lines. The finite-chain results reproduce all trends and features of the measured intensity, and together with the continuum bounds, suggest polarization assignments.

A more direct comparison is achieved by combining the calculations in Fig. 4(b) with results for $N = 24$, $m = 1/6$ and $N = 28$, $m = 1/7$, which correspond to $H = 9.18$ T and 8.21 T for CuPzN, respectively, and greatly increase the number of wavevectors sampled. The results at each N were smoothed by convolving them with the response function of a finite-size system, so that

$$\mathcal{S}_{\alpha\beta}(\tilde{q}, \hbar\omega) = \sum_N \sum_{\tilde{q}_N} \mathcal{S}_{\alpha\beta,N}(\tilde{q}_N, \hbar\omega) \left| \frac{\sin((\tilde{q} - \tilde{q}_N)N/2)}{\sin((\tilde{q} - \tilde{q}_N)/2)} \right|^2. \quad (1)$$

The calculated results were then converted to $\tilde{\mathcal{I}}_m(\tilde{q}, \omega)$ [6], and binned and averaged as described above. After multiplication by an overall scale factor, we obtain the contour plot shown in Fig. 4(c) which represents the measured intensity expected from an equal weighted ensemble of 24, 26, and 28 membered spin chains. While the relatively short chains yield stronger discrete energy bands than in the measurements, the simulation clearly captures the main features of the data.

Karbach and Müller have recently identified a new class of quasiparticles for the partially magnetized $S=1/2$ chain. These “psinons” play a similar role in the spectrum as do the spinons at $H = 0$, yielding a continuum for each component of $\mathcal{S}(\tilde{q}, \omega)$ [13, 14], with boundaries that are consistent with the approximate analytic expressions that were used above. Karbach *et al.* have computed the psinon lineshapes for $m = 0.25$, where $\tilde{q}_{i,1} = \tilde{q}_{i,2} = \pi/2$. This occurs at $H = 11.9$ T for CuPzN, but a qualitative comparison can still be made, as the properties of the lineshapes should vary smoothly. Of particular interest is the peak at the upper boundary of the psinon continuum for $\mathcal{S}_{zz}(\tilde{q}, \omega)$, which is due to a singularity in the psinon density of states. This may explain the line of scattering intensity in Fig. 4(a) that tracks the top of the \mathcal{E}_2 continuum. This is notably different from the zero-field case, where the corresponding singularity in the spinon density of states is compensated by a vanishing matrix element, and $\mathcal{S}(\tilde{q}, \omega)$ vanishes at the upper boundary of the spinon continuum, as seen in Fig. 1.

Finally, we note that Fig. 4(a) shows some evidence of weak scattering intensity for $\hbar\omega > 2$ meV. This could possibly be due to the presence of short chains resulting from impurities, or to higher-order processes not included in the spinon/psinon picture. However, we note that our error bars are much larger here than at lower energy due to shorter counting times, (see Fig. 2), and so a definitive statement on the existence of excitations in this energy range cannot be made at this time.

In summary, our experiments in CuPzN provide the first experimental example of an extended critical state in a quantum magnet. This detailed mapping of the spin excitation spectrum in the spin-1/2 linear chain antiferromagnet verifies long-standing predictions based on the Bethe Ansatz of a field driven and critical incommensurate state. There is excellent agreement with finite chain calculations, and good qualitative agreement with the lineshapes predicted at higher fields based on novel “psinon” quasiparticles. Recent advances in Bethe Ansatz techniques show promise for full calculations of the psinons’ contribution to $\mathcal{S}(\tilde{q}, \omega)$ [14, 24]. A direct comparison of such calculations to our data would clearly be very interesting.

This work was supported by NSF Grant No. DMR-0074571 and utilized facilities supported by NIST and the NSF under Agreement No. 9986442. X-ray characterization was carried out using facilities maintained by the JHU MRSEC under NSF Grant No. DMR-0080031.

-
- * Currently at Department of Physics, The Pennsylvania State University, University Park, Pennsylvania 16802
- [1] S. Sachdev, “Quantum Phase Transitions” Cambridge University Press (2000).
 - [2] D. A. Tennant *et al.*, Phys. Rev. B **52**, 13368 (1995).
 - [3] D. C. Dender *et al.*, Phys. Rev. B **53**, 2583 (1996).
 - [4] M. Takigawa *et al.*, Phys. Rev. Lett. **76**, 4612 (1996); Phys Rev. B. **56**, 13681 (1997).
 - [5] M. Arai *et al.*, Phys Rev. Lett. **77**, 3649 (1996).
 - [6] P. R. Hammar *et al.*, Phys. Rev. B **59**, 1008 (1999).
 - [7] G. Müller *et al.*, Phys. Rev. B **24**, 1429 (1981).
 - [8] M. Karbach *et al.*, Phys. Rev. B **55**, 12510 (1997).
 - [9] R. Chitra and T. Giamarchi, Phys. Rev. B **55**, 5816 (1997).
 - [10] N. M. Bogoliubov *et al.*, Nucl. Phys. B **275**, 687 (1986).
 - [11] A. Fledderjohann *et al.*, Phys. Rev. B **54**, 7168 (1996).
 - [12] K. Lefmann and C. Rischel, Phys. Rev. B **54**, 6340 (1996).
 - [13] M. Karbach and G. Müller, Phys. Rev. B **62**, 14871 (2000).
 - [14] M. Karbach *et al.*, Phys. Rev. B. **66**, 054405 (2002).
 - [15] D. C. Dender *et al.*, Phys. Rev. Lett. **79**, 1750 (1997).
 - [16] M. Oshikawa and I. Affleck, Phys. Rev. Lett. **79**, 2883 (1997); I. Affleck and M. Oshikawa, Phys. Rev. B **60**, 1038 (1999).
 - [17] D. B. Losee *et al.*, J. Chem. Phys. **59**, 3600 (1973); G. Mennenga *et al.*, J. Magn. Magn. Mater. **44**, 89 (1984); A. Santoro *et al.*, Acta Crystallogr., Sec. B **26**, 9979 (1970).
 - [18] M. B. Stone, Ph.D. Thesis, Johns Hopkins University, 2002.
 - [19] I. Zaliznyak, J. Appl. Phys. **91**, 8390 (2002).
 - [20] N. D. Chesser and J. D. Axe, Acta Crystallogr., Sect. A **29**, 160 (1973).
 - [21] A. H. Bougourzi *et al.*, Phys. Rev. B **54**, R12669 (1996).
 - [22] A. Fledderjohann *et al.*, Phys. Rev. B **53**, 11543 (1996).
 - [23] K. T. McGregor and S. G. Soos, J. Chem. Phys. **64**, 2506 (1976).
 - [24] D. Biegel *et al.*, Europhys. Lett. **59**, 882 (2002).